




Influence of effective nucleon mass on equation of state for supernova simulations and neutron stars

SHUYING LI,¹ JUNBO PANG,¹ HONG SHEN ¹, JINNIU HU ¹ AND KOHSUKE SUMIYOSHI ²

¹*School of Physics, Nankai University, Tianjin 300071, China*

²*National Institute of Technology, Numazu College, Shizuoka 410-8501, Japan*

ABSTRACT

We investigate the influence of effective nucleon mass on the equation of state (EOS), which is constructed for simulations of core-collapse supernovae and binary neutron-star mergers, within the relativistic mean-field (RMF) framework. The study introduces a new RMF parameter set, TM1m, which is a modification of the TM1e model with an adjusted effective mass, maintaining the saturation properties of nuclear matter. The TM1m model, with a larger effective mass ratio ($M^*/M \sim 0.8$) compared to the TM1e model ($M^*/M \sim 0.63$), is employed to construct a new EOS table, EOS5. This EOS table is designed to offer insights into the influence of effective nucleon mass on the EOS within a relativistic framework, particularly above the saturation density. The properties of cold neutron stars, calculated using the TM1m model, are compared with those of the TM1e and original TM1 models. Both the TM1m and TM1e models are found to be compatible with the latest constraints on tidal deformability and radii of neutron stars, derived from astrophysical observations.

Keywords: equation of state — supernovae: general — stars: neutron

1. INTRODUCTION

The equation of state (EOS) of hot and dense matter is an essential ingredient for understanding astrophysical phenomena, such as core-collapse supernovae, protoneutron star cooling, and binary neutron-star mergers (Oertel et al. 2017). The EOS should cover a wide range of temperature T , proton fraction Y_p , and baryon mass density ρ_B , which exhibits a complex phase diagram. At low temperatures and subsaturation densities, the matter is nonuniform where heavy nuclei are formed to lower the free energy of the system. When the density reaches about half of the nuclear saturation density, heavy nuclei tend to dissolve into a homogeneous nuclear liquid. At the density higher than 2-3 times the nuclear saturation density, non-nucleonic degrees of freedom such as hyperons and quarks may occur and soften the EOS of dense matter (Maruyama et al. 2007; Yasutake et al. 2014; Weber et al. 2019; Huang et al. 2022a,b; Sumiyoshi et al. 2023). On the other hand, with increasing temperature T , the density range of nonuniform matter shrinks, and

finally, heavy nuclei cannot be formed above a critical value of ~ 14 MeV (Shen et al. 2011b).

Owing to the complexity of the phase behavior of stellar matter, constructing a full EOS for general usage in astrophysical applications is a daunting task. A set of available EOSs has been summarized in the review by Oertel et al. (2017), which can also be obtained from the public database CompOSE (Typel et al. 2022). During the past decades, the two most commonly used EOSs in astrophysical simulations are the EOS of Lattimer & Swesty (1991) and that of Shen et al. (1998a). The Lattimer-Swesty EOS was based on the compressible liquid-drop (CLD) model with a non-relativistic Skyrme force. In contrast, the Shen EOS employed the relativistic mean-field (RMF) model and the Thomas-Fermi approximation with a parameterized nucleon distribution for the description of nonuniform matter. In these EOSs, the single nucleus approximation (SNA) was adopted, which meant that only a single representative nucleus was considered instead of an ensemble of nuclei. Recently, EOS tables were developed beyond the SNA by including multiple nuclei in nuclear statistical equilibrium (NSE) (Hempel & Schaffner-Bielich 2010; Furusawa et al. 2017a; Steiner et al. 2013; Schneider et al. 2017; Shen et al. 2011a; Raduta & Gulminelli 2019). It has been shown that considering the

shennankai@gmail.com

hujinniu@nankai.edu.cn

nuclear distributions may play an important role in the neutrino-matter interactions (Nagakura et al. 2019), but it has less influence on thermodynamic quantities of dense matter (Hempel & Schaffner-Bielich 2010). Furthermore, microscopic approaches based on realistic nuclear forces have also been used to construct the EOS table for astrophysical simulations (Togashi et al. 2017; Furusawa et al. 2017b, 2020).

The first version of Shen EOS (EOS1) was published in Shen et al. (1998a), in which we first provided the EOS in three-dimensional (T, Y_p, ρ_B) tabular form including the thermodynamic and compositional quantities needed in the applications. This EOS design is convenient for performing supernova simulations and has been commonly used in building EOS tables in subsequent years (Typel et al. 2015). In Shen et al. (2011b), we recalculated the EOS table with improved designs of ranges and grids, according to the requirements of EOS users. The improved EOS tables were referred to as: (a) EOS2, which includes only the nucleonic degree of freedom, and (b) EOS3, which incorporates additional Λ hyperons. Both EOS1 and EOS2 were based on the RMF approach using the TM1 parameterization for nuclear interactions. The nonuniform matter, consisting of a lattice of heavy nuclei, was described within the Thomas-Fermi approximation, in combination with assumed nucleon distribution functions and a free energy minimization procedure. The TM1 model provides a satisfactory description for finite nuclei and predicts a maximum neutron-star mass of $2.18M_\odot$ with nucleonic degrees of freedom only. However, the resulting neutron-star radii seem to be excessively large (Shen et al. 1998b, 2020). Remarkable progress in astrophysical observations has been achieved over the last decade, providing crucial constraints on the EOS of dense matter. A stringent constraint comes from the precise mass measurements of massive pulsars, PSR J1614-2230 ($1.908 \pm 0.016M_\odot$; Arzoumanian et al. (2018)), PSR J0348+0432 ($2.01 \pm 0.04M_\odot$; Antoniadis et al. (2013)), and PSR J0740+6620 ($2.08 \pm 0.07M_\odot$; Fonseca et al. (2021)), which require the predicted maximum neutron-star mass to be larger than $\sim 2M_\odot$. The first detection of gravitational waves from a binary neutron-star merger GW170817 (Abbott et al. 2017, 2018) provided an upper limit on the tidal deformability and constrained the radius of neutron stars (Fattoyev et al. 2018; Most et al. 2018). Furthermore, the recent observations by NICER (Neutron Star Interior Composition Explorer) for PSR J0030+0451 (Miller et al. 2019; Riley et al. 2019) and PSR J0740+6620 (Miller et al. 2021; Riley et al. 2021) provided simultaneous measurements of the mass and radius of neutron stars, which offer strong constraints

on the EOS of dense matter. Considering the progress in astrophysical observations, we constructed a revised version of the Shen EOS (EOS4) based on an extended TM1 model, referred to as the TM1e model, in Shen et al. (2020). It is noteworthy that the TM1e and original TM1 models have identical properties for symmetric nuclear matter, but exhibit different behaviors of the symmetry energy. The TM1e model has a symmetry energy slope of $L = 40$ MeV, significantly smaller than the value of $L = 111$ MeV in the original TM1 model. Consequently, it predicts smaller neutron-star radii, which are supported by astrophysical observations (Shen et al. 2020). By comparing the results from astrophysical simulations using EOS4 and EOS2, one can estimate the effects of symmetry energy and its density dependence (Sumiyoshi et al. 2019).

Recently, it was reported in Schneider et al. (2019); Yasin et al. (2020) that the effective nucleon mass has a decisive effect on supernova explosions through pressure difference, protoneutron star contraction, and neutrino emission (see also Andersen et al. (2021) for gravitational waves). A larger effective mass leads to smaller thermal contributions to the pressure, which results in a more rapid contraction and aids the shock evolution to a faster explosion. However, in their calculations, the influence of the effective mass was investigated using a set of Skyrme-type EOSs by varying the effective nucleon mass at saturation density, which was treated as a model parameter within a nonrelativistic framework. In Nakazato & Suzuki (2019), the influence of effective nucleon mass on the cooling process of a protoneutron star was investigated using a series of phenomenological EOSs, in which the effective nucleon mass, as a model parameter, was set to be constant. It is widely accepted that the effective mass should be density-dependent and can be incorporated more consistently in a relativistic framework than in nonrelativistic approaches.

In the present work, we will adjust the RMF parameters based on the TM1e parameterization, so that the saturation properties obtained by the new parameterization remain the same as those of TM1e, but with different effective masses. The TM1e model predicts an effective mass ratio $M^*/M \sim 0.63$ at the saturation density n_0 , while the new parameterization, referred to hereafter as the TM1m model, sets this ratio to be $M^*/M \sim 0.8$. Note that the effective masses in the TM1e and TM1 models are identical due to their same isoscalar properties. In order to investigate the impact of effective nucleon mass on astrophysical simulations, we construct a new EOS table (referred to as EOS5) using the TM1m model. We prepare all quantities in the EOS table for uniform matter at densities higher

than $\sim 10^{14}$ g/cm³ by using the TM1m model, which can then be combined with nonuniform part of Shen EOS4 at low densities to generate the final EOS table, as often done in the literature [Ishizuka et al. \(2008\)](#); [Sumiyoshi et al. \(2019\)](#). By switching only the uniform matter in EOS5 with the TM1m model, we clarify the influence of effective mass at high densities. The application of EOS5 with $M^*/M \sim 0.8$, compared to EOS4 with $M^*/M \sim 0.63$, can be used to clarify the impact of effective mass on astrophysical simulations such as core-collapse supernovae, protoneutron star cooling, and binary neutron-star mergers.

This paper is arranged as follows. In Section 2, we briefly describe the RMF approach used for constructing the EOS table, and compare different parameter sets. In Section 3, we present numerical results using the new parameterization TM1m and compare them to the results from the TM1e and original TM1 models. Finally, a summary and conclusions are presented in Section 4.

2. MODEL AND PARAMETERS

In order to make the article self-contained, we give a brief description of the RMF model used for constructing the EOS table. We employ the RMF model, including nonlinear terms for the σ and ω mesons, and an additional ω - ρ coupling term. Nucleons interact through the exchange of mesons, specifically scalar σ , vector ω , and isovector ρ mesons ([Bao et al. 2014](#); [Shen et al. 2020](#)). The nucleonic Lagrangian density can be expressed as

$$\begin{aligned} \mathcal{L}_{\text{RMF}} = & \sum_{i=p,n} \bar{\psi}_i [i\gamma_\mu \partial^\mu - (M + g_\sigma \sigma) \\ & - \gamma_\mu \left(g_\omega \omega^\mu + \frac{g_\rho}{2} \tau_a \rho^{a\mu} \right)] \psi_i \\ & + \frac{1}{2} \partial_\mu \sigma \partial^\mu \sigma - \frac{1}{2} m_\sigma^2 \sigma^2 - \frac{1}{3} g_2 \sigma^3 - \frac{1}{4} g_3 \sigma^4 \\ & - \frac{1}{4} W_{\mu\nu} W^{\mu\nu} + \frac{1}{2} m_\omega^2 \omega_\mu \omega^\mu + \frac{1}{4} c_3 (\omega_\mu \omega^\mu)^2 \\ & - \frac{1}{4} R_{\mu\nu}^a R^{a\mu\nu} + \frac{1}{2} m_\rho^2 \rho_\mu^a \rho^{a\mu} \\ & + \Lambda_v (g_\omega^2 \omega_\mu \omega^\mu) (g_\rho^2 \rho_\mu^a \rho^{a\mu}), \end{aligned} \quad (1)$$

where $W^{\mu\nu}$ and $R^{a\mu\nu}$ represent the antisymmetric field tensors corresponding to ω^μ and $\rho^{a\mu}$, respectively. Within the mean-field approximation, the meson field operators are replaced by their expectation values. In a static uniform system, the nonzero components are given by $\sigma = \langle \sigma \rangle$, $\omega = \langle \omega^0 \rangle$, and $\rho = \langle \rho^{30} \rangle$. The equations of motion for nucleons and mesons are derived from the Lagrangian density, and these coupled equations can be solved self-consistently within the RMF framework.

In order to explore the influence of effective nucleon mass on astrophysical simulations, we refit the RMF parameters based on the TM1e model used in constructing

the Shen EOS4 ([Shen et al. 2020](#)). A new parameter set, referred to as TM1m, is introduced with a larger effective mass, while all other saturation properties remain identical to those of TM1e. In Table 1, we present the coupling constants of the TM1m, TM1e, and original TM1 models, while the corresponding saturation properties are listed in Table 2. It is shown that the main difference between TM1m and TM1e is the effective mass, i.e., $M^*/M \sim 0.8$ in the TM1m model and $M^*/M \sim 0.63$ in the TM1e model. On the other hand, the difference between TM1e and TM1 lies in the density dependence of symmetry energy, with the symmetry energy slope being $L = 40$ MeV in the TM1e model and $L = 111$ MeV in the original TM1 model, respectively.

In Figure 1, we plot the energy per baryon E/A of symmetric nuclear matter and neutron matter as a function of the baryon number density n_B . It is shown that the behaviors of symmetric nuclear matter are exactly the same between the TM1e and TM1 models, whereas those of the TM1m model are slightly lower as the density increases. This is because the larger effective mass in the TM1m model leads to a smaller kinetic energy. Moreover, the TM1m model exhibits less attraction by σ meson and weaker repulsion by ω meson, compared to the TM1e and TM1 models. Relativistic effects are well-known to increase with density, which can yield relatively smaller kinetic energy for particles with larger mass, especially at higher densities. There are significant differences in neutron matter between these three models. This is related to different density dependence of symmetry energy and relativistic effects.

In Figure 2, we show the effective nucleon mass M^* as a function of the baryon number density n_B . It is seen that the TM1e model maintains the exact same behavior for M^* as the original TM1 model, whereas M^* in the TM1m model is notably larger than that in TM1. The effective mass is known to play a key role in neutrino emission processes ([Yasin et al. 2020](#)), which motivates us to explore the effects caused by the effective mass on the realistic EOS table. On the other hand, the effective mass is closely related to the spin-orbit splittings in finite nuclei, namely, a larger Dirac mass corresponds to a smaller spin-orbit splitting. The behavior of spin-orbit splittings can be improved by introducing an additional tensor interaction, which does not contribute to uniform matter at high densities ([Typel & Alvear Terrero 2020](#)).

In Figure 3, we display the symmetry energy E_{sym} as a function of the baryon number density n_B . At higher densities, E_{sym} in the TM1e model is lower than that in the original TM1 model. This is because the TM1e model has a relatively smaller slope parameter ($L = 40$ MeV) than the TM1 model ($L = 111$ MeV). On the

other hand, E_{sym} in the TM1m model is slightly lower than that in the TM1e model, which is more evident with increasing density. Although the TM1m model has the same slope parameter ($L = 40$ MeV) as the TM1e model, its larger effective mass, together with the smaller coupling constants g_σ and g_ω , can reduce the relativistic effects and lead to smaller E_{sym} at higher densities. It is noteworthy that these three models have the same values of E_{sym} at a density of 0.11 fm^{-3} . This is because the model parameters are chosen to keep E_{sym} fixed at the density of 0.11 fm^{-3} . This choice is due to the fact that binding energies of finite nuclei are essentially determined by the symmetry energy at a density of 0.11 fm^{-3} , not by the symmetry energy at saturation density (Bao et al. 2014; Zhang & Chen 2013).

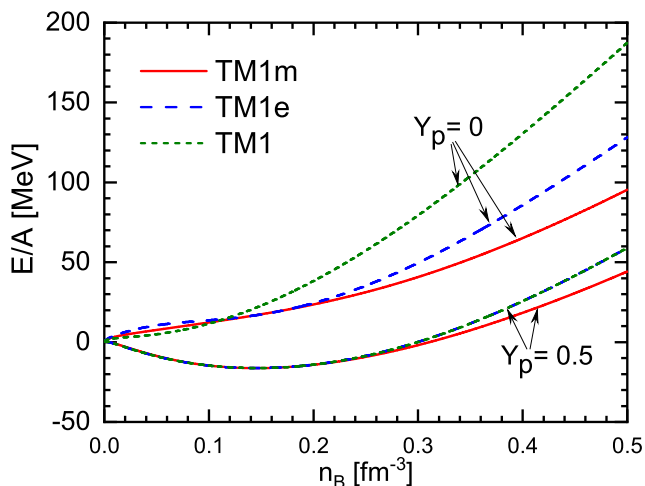


Figure 1. Energy per baryon E/A of symmetric nuclear matter and neutron matter as a function of the baryon number density n_B in the RMF models.

To construct a realistic EOS table for general usage in astrophysical simulations, we should perform calculations covering a wide range of temperature T , proton fraction Y_p , and baryon mass density ρ_B . For uniform nuclear matter at densities above $\sim 10^{14} \text{ g/cm}^3$, all required quantities can be derived within the RMF framework. To ensure completeness, we present the key thermodynamic quantities of uniform nuclear matter: energy density ϵ , entropy density s , and pressure p . The energy density in the TM1m model is given by

$$\begin{aligned} \epsilon = & \sum_{i=p,n} \frac{1}{\pi^2} \int_0^\infty dk k^2 \sqrt{k^2 + M^{*2}} (f_{i+}^k + f_{i-}^k) \\ & + \frac{1}{2} m_\sigma^2 \sigma^2 + \frac{1}{3} g_2 \sigma^3 + \frac{1}{4} g_3 \sigma^4 + \frac{1}{2} m_\omega^2 \omega^2 \\ & + \frac{3}{4} c_3 \omega^4 + \frac{1}{2} m_\rho^2 \rho^2 + 3\Lambda_v (g_\omega^2 \omega^2) (g_\rho^2 \rho^2), \end{aligned} \quad (2)$$

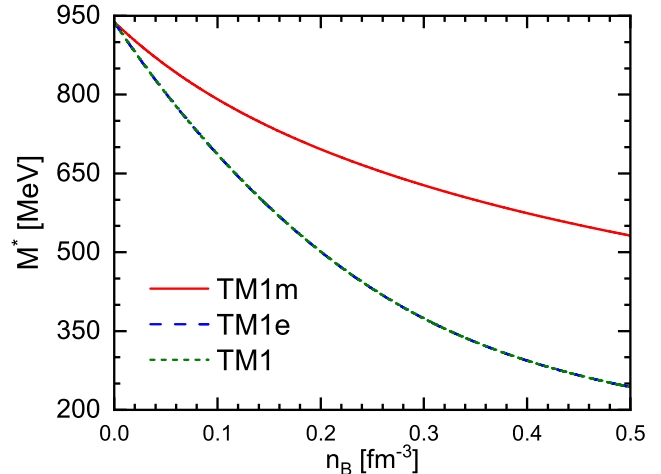


Figure 2. Effective nucleon mass M^* as a function of the baryon number density n_B in the RMF models.

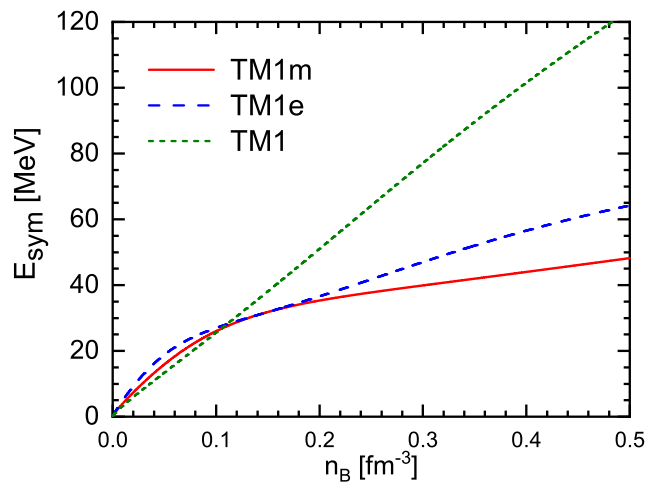


Figure 3. Symmetry energy E_{sym} as a function of the baryon number density n_B in the RMF models.

the entropy density is written as

$$\begin{aligned} s = & - \sum_{i=p,n} \frac{1}{\pi^2} \int_0^\infty dk k^2 [f_{i+}^k \ln f_{i+}^k + (1 - f_{i+}^k) \ln (1 - f_{i+}^k) \\ & + f_{i-}^k \ln f_{i-}^k + (1 - f_{i-}^k) \ln (1 - f_{i-}^k)], \end{aligned} \quad (3)$$

and the pressure is given by

$$\begin{aligned} p = & \sum_{i=p,n} \frac{1}{3\pi^2} \int_0^\infty dk k^2 \frac{k^2}{\sqrt{k^2 + M^{*2}}} (f_{i+}^k + f_{i-}^k) \\ & - \frac{1}{2} m_\sigma^2 \sigma^2 - \frac{1}{3} g_2 \sigma^3 - \frac{1}{4} g_3 \sigma^4 + \frac{1}{2} m_\omega^2 \omega^2 \\ & + \frac{1}{4} c_3 \omega^4 + \frac{1}{2} m_\rho^2 \rho^2 + \Lambda_v (g_\omega^2 \omega^2) (g_\rho^2 \rho^2). \end{aligned} \quad (4)$$

Here, $M^* = M + g_\sigma \sigma$ denotes the effective nucleon mass. f_{i+}^k and f_{i-}^k ($i = p, n$) are the occupation probabilities

Table 1. Coupling constants of the TM1m, TM1e, and original TM1 models.

Model	g_σ	g_ω	g_ρ	g_2 [fm ⁻¹]	g_3	c_3	Λ_v
TM1m	7.93528	8.63169	11.51296	-11.51628	54.88715	0.00025	0.09326
TM1e	10.0289	12.6139	13.9714	-7.2325	0.6183	71.3075	0.0429
TM1	10.0289	12.6139	9.2644	-7.2325	0.6183	71.3075	0.0000

Table 2. Nuclear matter properties obtained in the TM1m, TM1e, and original TM1 models. The saturation density and the energy per particle are denoted by n_0 and E/A , the incompressibility by K , the symmetry energy and its slop by E_{sym} and L , the effective mass ratio by M^*/M .

Model	n_0 (fm ⁻³)	E/A (MeV)	K (MeV)	E_{sym} (MeV)	L (MeV)	M^*/M
TM1m	0.145	-16.3	281	31.4	40	0.793
TM1e	0.145	-16.3	281	31.4	40	0.634
TM1	0.145	-16.3	281	36.9	111	0.634

of nucleon and antinucleon at momentum k , which are given by the Fermi-Dirac distribution,

$$f_{i\pm}^k = \left\{ 1 + \exp \left[\left(\sqrt{k^2 + M^{*2}} \mp \nu_i \right) / T \right] \right\}^{-1}. \quad (5)$$

The kinetic part of the chemical potential ν_i is related to the chemical potential μ_i as

$$\mu_i = \nu_i + g_\omega \omega + \frac{g_\rho}{2} \tau_{3i} \rho. \quad (6)$$

The number density of protons ($i = p$) or neutrons ($i = n$) can be obtained by

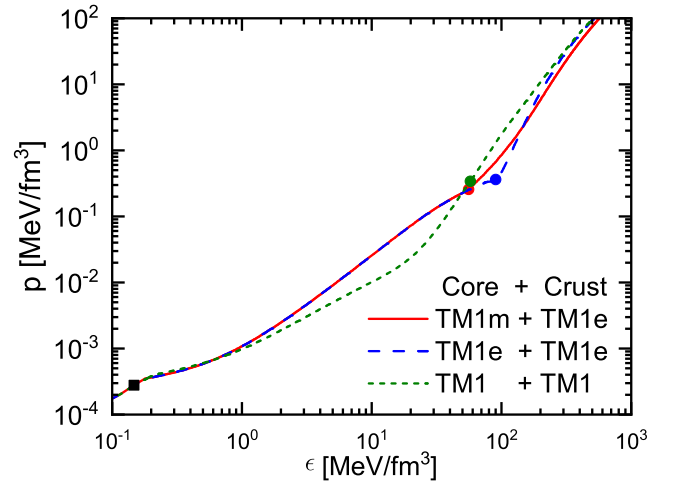
$$n_i = \frac{1}{\pi^2} \int_0^\infty dk k^2 (f_{i+}^k - f_{i-}^k). \quad (7)$$

The free energy density is given by $f = \epsilon - Ts$. Within the RMF model for uniform matter, these thermodynamic quantities satisfy the self-consistent relation:

$$f = \sum_{i=p,n} \mu_i n_i - p. \quad (8)$$

3. RESULTS AND DISCUSSION

In this section, we present numerical results using the TM1m model with a larger effective mass, and meanwhile make an in-depth comparison with the TM1e and original TM1 models. First, we discuss the properties of neutron stars at zero temperature and check the compatibility with current observations. Second, we show the results of the new EOS table (EOS5), especially at densities higher than $\sim 10^{14}$ g/cm³, in order to explore the impact of effective nucleon mass on the EOS table.

**Figure 4.** Pressure p as a function of the energy density ϵ obtained using the TM1m, TM1e, and original TM1 models for the core. The BPS EOS is adopted for the outer crust and the matching point is marked by the filled square. The inner crust is described in the Thomas-Fermi approximation using the TM1e and TM1 models. The crust-core transition is indicated by the filled circles.

3.1. Neutron stars at zero temperature

The properties of static neutron stars can be obtained by solving the well-known Tolman-Oppenheimer-Volkoff (TOV) equation with the EOS over a wide range of densities. The neutron star matter is assumed to be in beta equilibrium with charge neutrality at zero temperature. Generally, the EOS used for the calculations of neutron star structure can be divided into at least three segments: (a) the EOS of the outer crust below the neutron drip density; (b) the EOS of the inner crust

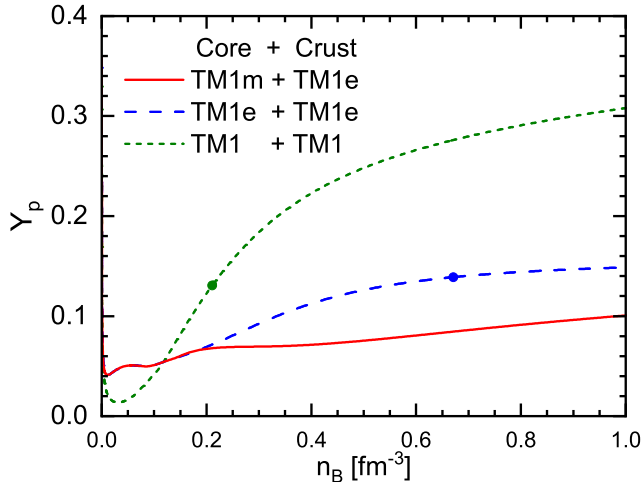


Figure 5. Proton fraction Y_p as a function of the baryon density n_B for the TM1m, TM1e, and the TM1 models. The filled circles indicate the threshold for the dUrca process.

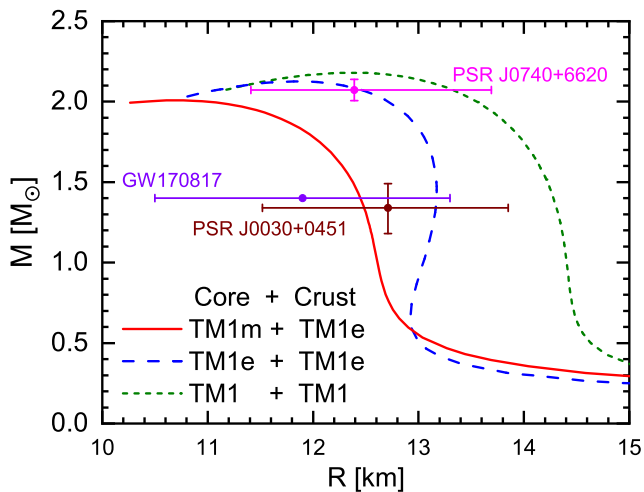


Figure 6. Mass-radius relations of neutron stars obtained using the EOS shown in Figure 4. The horizontal violet line represents the constraint on $R_{1.4}$ inferred from GW170817 (Abbott et al. 2018). The horizontal brown and magenta lines correspond to simultaneous measurements of the mass and radius from NICER for PSR J0030+0451 (Riley et al. 2019) and PSR J0740+6620 (Riley et al. 2021), respectively.

from neutron drip to crust-core transition; (c) the EOS of the liquid core above the crust-core transition. In the present work, we use the Baym-Pethick-Sutherland (BPS) EOS (Baym et al. 1971) for the outer crust, while the inner crust EOS is based on the self-consistent Thomas-Fermi approximation using both TM1e ($L = 40$ MeV) and TM1 ($L = 111$ MeV) parameterizations (Ji et al. 2019). The EOS of the liquid core above the crust-

core transition is calculated in the RMF approach using the TM1m, TM1e, and TM1 parameterizations. In Figure 4, we show the pressure p as a function of the energy density ϵ . It is shown that the TM1m model predicts relatively small pressures at high densities, while the TM1 EOS is stiffer than other two cases. The EOSs with TM1e (blue dashed line) and TM1 (green dotted line) are unified EOSs, because their inner crust and core segments are obtained within the same nuclear model. The TM1m core EOS is connected to the TM1e inner crust EOS at their crossing point.

In Figure 5, the proton fraction Y_p is plotted as a function of the baryon density n_B , and the corresponding threshold density for the dUrca process is indicated by the filled circles. It is well-known that the dUrca process can occur for $Y_p \geq 1/9$ in a simple npe matter, while the critical Y_p for the dUrca process is in the range of $(11.1 - 14.8)\%$ when the muons are included under the equilibrium condition $\mu_e = \mu_\mu$ (Lattimer et al. 1991). The original TM1 model ($L = 111$ MeV) predicts higher Y_p and smaller dUrca threshold density ($\sim 0.21 \text{ fm}^{-3}$). The curve of TM1e is lower than that of TM1, while its dUrca threshold density is about 0.67 fm^{-3} . In the case of TM1m, the values of Y_p are much lower than that in the TM1 and TM1e model, which is caused by its smaller symmetry energies at higher densities, as shown in Figure 3. Therefore, the critical Y_p for the dUrca process could not be reached in the TM1m model.

In Figure 6, we display the predicted mass-radius relations of neutron stars using the EOSs from Figure 4, along with several constraints from astrophysical observations. It is found that the maximum masses of neutron stars predicted by the TM1m, TM1e, and TM1 models are about 2.01 , 2.12 , and $2.18 M_\odot$, respectively, which fulfill the observational constraints on the maximum mass $M_{\text{max}} > 2 M_\odot$. The mass-radius relations exhibit significant variations among these models, which are caused by different behaviors of the symmetry energy and its slope, as shown in Figure 3. For the radius of a canonical $1.4 M_\odot$ neutron star, denoted as $R_{1.4}$, a large value of ~ 14.2 km is obtained using the TM1 model, while it reduces to 13.1 km in the TM1e model and 12.4 km in the TM1m models, respectively. The analysis of GW170817 data provides a constraint on $R_{1.4}$, with an estimated value of $R_{1.4} = 11.9 \pm 1.4$ km (Abbott et al. 2018). The resulting $R_{1.4}$ within the TM1m and TM1e models can be compatible with the constraint inferred from GW170817.

The observation of gravitational waves from GW170817 has provided valuable insights and constraints on the tidal deformability of neutron stars. Theoretically, the tidal deformability Λ can be calcu-

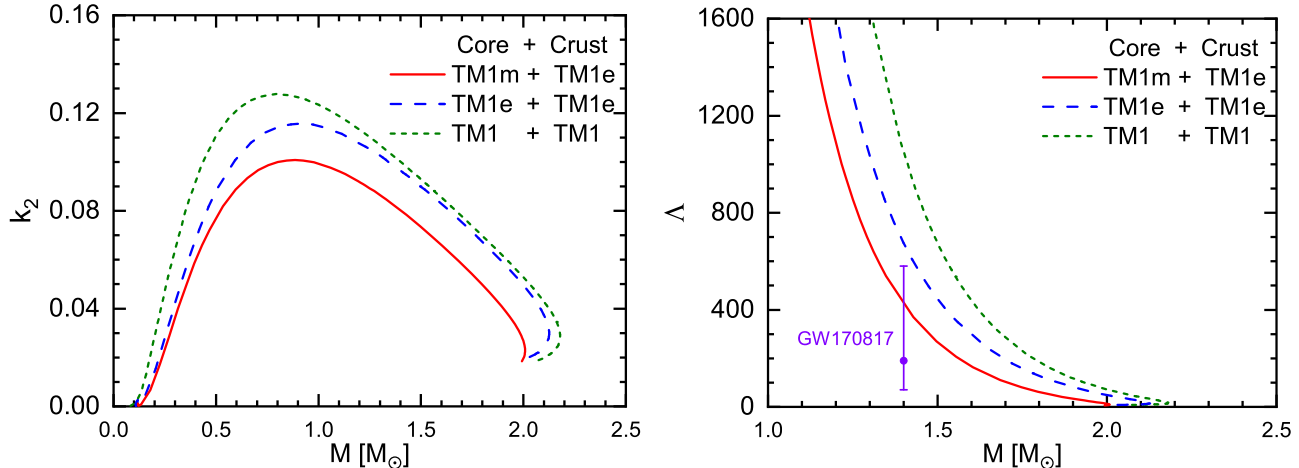


Figure 7. Love number k_2 and tidal deformability Λ as a function of the neutron-star mass M obtained using the EOS shown in Figure 4. The vertical violet line represents the constraint on $\Lambda_{1.4}$ inferred from GW170817 (Abbott et al. 2018).

lated using the EOS through both the tidal Love number k_2 and the compactness parameter $C = M/R$, following the relation $\Lambda = \frac{2}{3}k_2C^{-5}$ (Ji et al. 2019). In Figure 7, we show the tidal Love number k_2 (left panel) and the dimensionless tidal deformability Λ (right panel) as a function of the neutron-star mass M . It is observed that k_2 rises as the neutron-star mass increases, achieving its maximum at a mass of around 0.7 to 0.9 M_\odot . Subsequently, in the more massive range, k_2 exhibits a rapid reduction. It is noticeable that the TM1m model predicts a smaller k_2 value compared to the TM1e and TM1 models, which leads to a lower tidal deformability Λ within the TM1m model, as illustrated in the right panel of Figure 7. Generally, the value of Λ is very large for a small neutron-star mass due to its small compactness parameter C . As the star mass increases, the tidal deformability Λ decreases rapidly. The analysis of GW170817 has provided a constraint on the tidal deformability of a $1.4M_\odot$ neutron star, i.e., $70 \leq \Lambda_{1.4} \leq 580$ (Abbott et al. 2018). The resulting $\Lambda_{1.4}$ in the TM1m model is compatible with the constraint inferred from the analysis of GW170817.

3.2. Supernova matter at finite temperature

To explore the influence of effective nucleon mass on astrophysical simulations such as core-collapse supernovae and binary neutron-star mergers, we construct a new EOS table (EOS5) using the TM1m model. All quantities listed in the EOS table, as detailed in Appendix A of Shen et al. (2011b), are calculated using the TM1m model for uniform matter at densities higher than $\sim 10^{14}$ g/cm³, which can then be combined with nonuniform part of Shen EOS4 at low densities to generate the final EOS table, as often done in the literature Ishizuka et al. (2008); Sumiyoshi et al. (2019). As

illustrated in Figures 1-3, the discrepancies between the TM1m and TM1e models become increasingly evident as the density increases. Consequently, our analysis focuses on a detailed comparison of uniform matter at high densities. There will be a separate work on the low density part of EOS table elsewhere.

The EOS table covers a wide range of temperature T , proton fraction Y_p , and baryon mass density ρ_B for use in numerical simulations of core-collapse supernovae, protoneutron star cooling, and binary neutron-star mergers. For convenience in practical use, we provide the EOS table in the same tabular form as given in Table 1 of Shen et al. (2011b), which has been extensively adopted by the EOSs posted on the public database CompOSE. In general, when the temperature is higher than a critical value of ~ 14 MeV and the density is beyond $\sim 10^{14.1}$ g/cm³, heavy nuclei dissolve and the favorable state is uniform nuclear matter. In Figure 8, we display the effective nucleon mass M^* as a function of the baryon mass density ρ_B at $T = 1$ and 10 MeV. Although the calculations are performed at $Y_p = 0.5$, the results of M^* are found to be insensitive to Y_p . This is because M^* is determined by the scalar meson σ according to the relation $M^* = M + g_\sigma\sigma$. Notably, the effective masses in the TM1e and TM1 models are identical due to their same isoscalar properties. The results obtained in the TM1m model (red solid lines) are significantly larger than those of TM1e (blue dashed lines) and TM1 (green dotted lines). It is shown that M^* decreases as the density increases. At the saturation density n_0 ($\rho_B \simeq 10^{14.4}$ g/cm³), the effective masses obtained in the TM1m and TM1e models are, respectively, $M^* = 744$ MeV and $M^* = 595$ MeV. When the density rises to $\rho_B = 10^{15}$ g/cm³ (about $4n_0$), the effective masses decrease to $M^* = 496$ MeV in the TM1m model

and $M^* = 210$ MeV in the TM1e model, respectively. Comparing the case at $T = 10$ MeV in the upper panel with that at $T = 1$ MeV in the lower panel, the behaviors of the effective masses are similar. This suggests that the effective mass has a rather weak dependence on temperature.

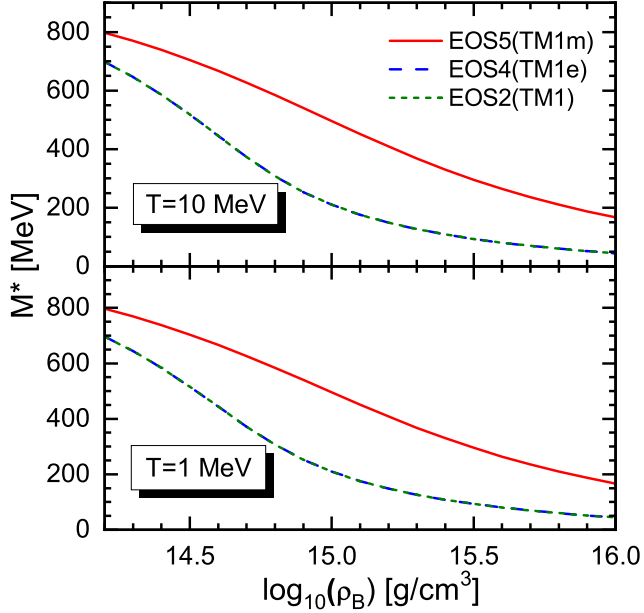


Figure 8. Effective nucleon mass M^* as a function of the baryon mass density ρ_B at $T = 1$ and 10 MeV. The results obtained in the TM1m model are compared with those of the TM1e and TM1 models.

It is essential to investigate how the effective mass influences the thermodynamic quantities within the EOS table. In Figure 9, we plot the free energy per baryon F as a function of the baryon mass density ρ_B for $Y_p = 0.1$ and 0.5 at $T = 1$ and 10 MeV. The results in EOS5(TM1m) are compared with those in EOS4(TM1e) and EOS2(TM1). At densities below $\rho_B \simeq 10^{15.4}$ g/cm³ (about $10n_0$), the free energies in the TM1m model are lower than those in the TM1e model, which can be more easily observed in Figure 1. This is because the larger effective mass in the TM1m model leads to a relatively smaller kinetic energy. However, at extremely high densities, the free energies in the TM1m model exceed those in the TM1e model, owing to the growing contributions from nonlinear meson terms. As for the dependence on Y_p , it is noteworthy that the differences between the results of $Y_p = 0.5$ and $Y_p = 0.1$ are clearly model-dependent. The differences in the TM1m and TM1e models are similar, but much smaller than those in the TM1 model. This is because the TM1 model exhibits significantly larger symmetry energies at higher densities, as shown in Figure 3. Comparing the free energy

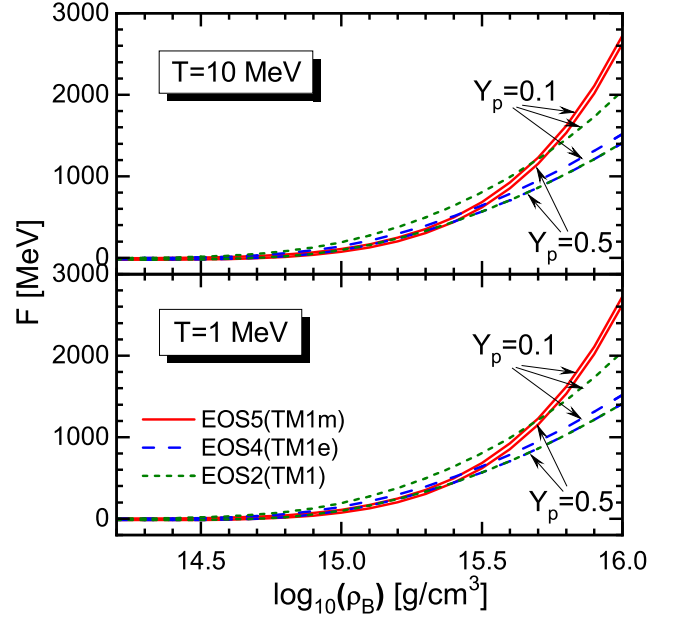


Figure 9. Free energy per baryon F as a function of the baryon mass density ρ_B with $Y_p = 0.1$ and 0.5 at $T = 1$ and 10 MeV. The results obtained in the TM1m model are compared with those of the TM1e and TM1 models.

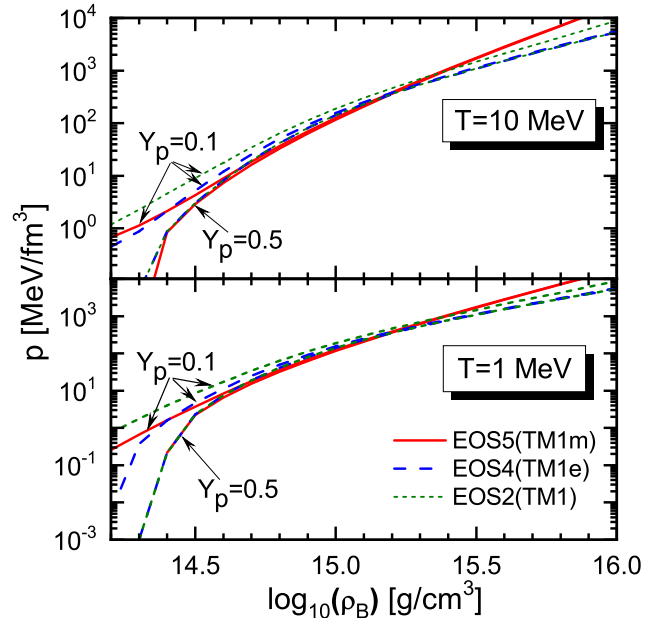


Figure 10. Same as Figure 9, but for the pressure p .

trends between $T = 1$ MeV and $T = 10$ MeV, it is observed that they are very similar.

In Figure 10, we display the pressure p as a function of ρ_B for $Y_p = 0.1$ and 0.5 at $T = 1$ and 10 MeV. The pressure of uniform nuclear matter is calculated within the RMF framework by Equation (4).

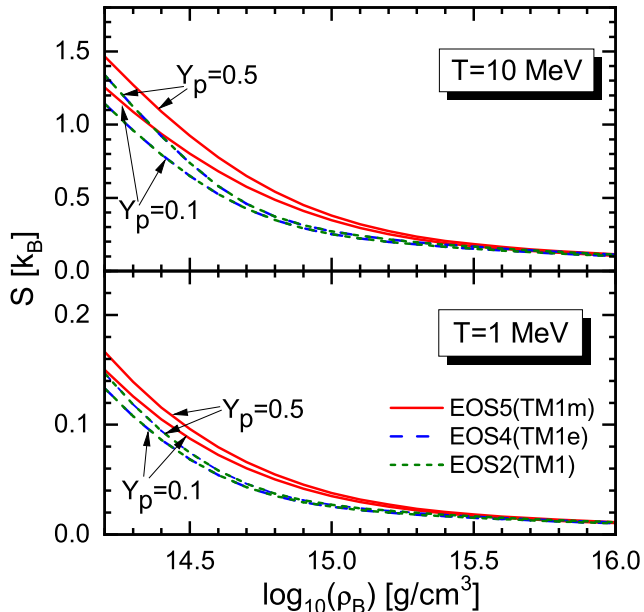


Figure 11. Same as Figure 9, but for the entropy per baryon S .

According to tradition, when constructing EOS table, the contributions from leptons and photons are usually calculated separately, which are not included in the present work. As shown in Figure 10, it is evident that at low densities, the pressure values are very small, even reaching negative levels when $Y_p = 0.5$. It is known that the pressure of leptons and photons is significantly higher than that of baryons around the saturation density, and the total pressure becomes positive when the contributions from leptons and photons are taken into account. With increasing density, the pressure rises rapidly. The discrepancies between the TM1m and TM1e models are density-dependent. At densities below $\rho_B \simeq 10^{15.2} \text{ g/cm}^3$, the pressures in the TM1m model are lower than those in the TM1e model, due to the relatively large effective mass in the TM1m model. At extremely high densities, the pressure values in the TM1m model exceed those in the TM1e model. This is due to the increasing influence of nonlinear meson terms.

In Figure 11, we show the entropy per baryon S as a function of ρ_B for $Y_p = 0.1$ and 0.5 at $T = 1$ and 10 MeV. It can be seen that the values of S significantly decrease with increasing density. There are noticeable differences between the TM1m and TM1e models, whereas the results in the TM1 model are almost identical to those of TM1e. From Equations (3) and (5), it is seen that the entropy S is closely related to the effective mass M^* . The discrepancies between these models can be understood by analyzing the behaviors of M^* , as shown in Figure 8. On the other hand, the difference of symmetry

energy between TM1e and TM1 models has minor influence on the entropy. It is worth noting that the entropy values at $T = 10$ MeV (upper panel) are roughly ten times greater than those of $T = 1$ MeV (lower panel). Generally, the differences between $Y_p = 0.1$ and 0.5 decrease as the density increases.

4. SUMMARY

In this work, we investigated the influence of effective nucleon mass on the EOS for astrophysical simulations such as core-collapse supernovae, protoneutron star cooling, and binary neutron-star mergers. We employed the RMF model, in which the effective nucleon mass is more consistently integrated than it is in non-relativistic approaches such as the Skyrme model. A new RMF parameter set, TM1m, was introduced in the present work, which is a modification of the TM1e parameterization with a larger effective mass. The TM1m model preserves the same saturation properties as the TM1e model, but their effective masses are significantly different: $M^*/M \sim 0.8$ for the TM1m model and $M^*/M \sim 0.63$ for the TM1e model. It is well-known that there exists a positive correlation between the symmetry energy slope L and the neutron-star radius. In contrast to the original TM1 model characterized by $L = 111$ MeV, both the TM1m and TM1e models provide a small value of $L = 40$ MeV, which is more favored by recent astrophysical observations.

We calculated the properties of cold neutron stars using the TM1m model, and compared with the results obtained by the TM1e and TM1 models. The maximum masses of neutron stars obtained in these models could fulfill the observational constraint $M_{\text{max}} > 2 M_\odot$. It was found that the mass-radius relations exhibited significant variations among these models, which might be mainly caused by different behaviors of symmetry energy and its slope. Regarding the radius of a canonical $1.4 M_\odot$ neutron star ($R_{1.4}$), a large value of ~ 14.2 km was obtained using the TM1 model, while it reduced to 13.1 km in the TM1e model and 12.4 km in the TM1m models, respectively. The resulting radius $R_{1.4}$ and the tidal deformability $\Lambda_{1.4}$ within the TM1m model could be compatible with the constraint inferred from the gravitational wave event GW170817.

To explore the impact of effective nucleon mass in astrophysical simulations such as core-collapse supernovae and binary neutron-star mergers, we constructed a new EOS table (EOS5) using the TM1m model. All quantities included in the EOS table were calculated using the TM1m model for uniform matter at densities higher than $\sim 10^{14} \text{ g/cm}^3$, which could be combined with nonuniform part of Shen EOS4 at low densities

to generate the final EOS table. It was shown that the effective nucleon mass M^* significantly decreases as the density increases. At supra-saturation densities, the TM1m model predicts lower free energies and pressures than the TM1e model, which may be due to the fact that larger effective masses in the TM1m model result in relatively smaller kinetic energies. However, at extremely high densities, the free energies in the TM1m model exceed those in the TM1e model, owing to the growing contributions from nonlinear meson terms. We conclude that the effective nucleon mass plays an important role in the EOS for astrophysical simulations. The new EOS table (EOS5) constructed using the TM1m model offers a valuable resource to explore the influence of effective nucleon mass on the dynamics of supernovae. Numerical simulations of core-collapse supernovae, as well as analyses of the influence of effective nucleon mass, are currently underway.

5. ACKNOWLEDGMENTS

This work was supported in part by the National Natural Science Foundation of China (Grant No.

12175109), and the Natural Science Foundation of Guangdong Province (Grant No: 2024A1515010911). KS is supported by Grant-in-Aid for Scientific Research (19K03837, 20H01905,24K00632) from the Ministry of Education, Culture, Sports, Science and Technology (MEXT), Japan. KS acknowledges Computing Research Center, KEK, JLDG on SINET of NII, Research Center for Nuclear Physics, Osaka University, Yukawa Institute of Theoretical Physics, Kyoto University, Nagoya University, and Information Technology Center, University of Tokyo for providing high performance computing resources. KS is partly supported by MEXT as “Program for Promoting Researches on the Supercomputer Fugaku” (Structure and Evolution of the Universe Unraveled by Fusion of Simulation and AI, JPMXP1020230406, Project ID: hp230204, hp230270, hp240219, hp240264), the HPCI System Research Project (Project ID: hp230056, hp240041) and the Particle, Nuclear and Astro Physics Simulation Program (No. 2023-003) of Institute of Particle and Nuclear Studies, High Energy Accelerator Research Organization (KEK).

REFERENCES

- Abbott, B. P., Abbott, R., Abbott, T., et al. 2017, *Physical Review Letters*, 119, 161101
- . 2018, *Physical Review Letters*, 121, 161101, doi: [10.1103/PhysRevLett.121.161101](https://doi.org/10.1103/PhysRevLett.121.161101)
- Andersen, O. E., Zha, S., da Silva Schneider, A., et al. 2021, *The Astrophysical Journal*, 923, 201, doi: [10.3847/1538-4357/ac294c](https://doi.org/10.3847/1538-4357/ac294c)
- Antoniadis, J., Freire, P. C. C., Wex, N., et al. 2013, *Science*, 340, 1233232, doi: [10.1126/science.1233232](https://doi.org/10.1126/science.1233232)
- Arzoumanian, Z., Brazier, A., Burke-Spolaor, S., et al. 2018, *The Astrophysical Journal Supplement Series*, 235, 37, doi: [10.3847/1538-4365/aab5b0](https://doi.org/10.3847/1538-4365/aab5b0)
- Bao, S., Hu, J., Zhang, Z., & Shen, H. 2014, *Physical Review C*, 90, 045802, doi: [10.1103/PhysRevC.90.045802](https://doi.org/10.1103/PhysRevC.90.045802)
- Baym, G., Bethe, H. A., & Pethick, C. J. 1971, *Nuclear Physics A*, 175, 225, doi: [https://doi.org/10.1016/0375-9474\(71\)90281-8](https://doi.org/10.1016/0375-9474(71)90281-8)
- Fattoyev, F. J., Piekarewicz, J., & Horowitz, C. J. 2018, *Physical Review Letters*, 120, 172702, doi: [10.1103/PhysRevLett.120.172702](https://doi.org/10.1103/PhysRevLett.120.172702)
- Fonseca, E., Cromartie, H. T., Pennucci, T. T., et al. 2021, *The Astrophysical Journal Letters*, 915, L12, doi: [10.3847/2041-8213/ac03b8](https://doi.org/10.3847/2041-8213/ac03b8)
- Furusawa, S., Sumiyoshi, K., Yamada, S., & Suzuki, H. 2017a, *Nuclear Physics A*, 957, 188, doi: <https://doi.org/10.1016/j.nuclphysa.2016.09.002>
- Furusawa, S., Togashi, H., Nagakura, H., et al. 2017b, *Journal of Physics G: Nuclear and Particle Physics*, 44, 094001
- Furusawa, S., Togashi, H., Sumiyoshi, K., et al. 2020, *Progress of Theoretical and Experimental Physics*, 2020, 013D05, doi: [10.1093/ptep/ptz135](https://doi.org/10.1093/ptep/ptz135)
- Hempel, M., & Schaffner-Bielich, J. 2010, *Nuclear Physics A*, 837, 210, doi: <https://doi.org/10.1016/j.nuclphysa.2010.02.010>
- Huang, K., Hu, J., Zhang, Y., & Shen, H. 2022a, *The Astrophysical Journal*, 935, 88, doi: [10.3847/1538-4357/ac7f3c](https://doi.org/10.3847/1538-4357/ac7f3c)
- . 2022b, *Nuclear Physics Review*, 39, 135, doi: [10.11804/NuclPhysRev.39.2022013](https://doi.org/10.11804/NuclPhysRev.39.2022013)
- Ishizuka, C., Ohnishi, A., Tsubakihara, K., Sumiyoshi, K., & Yamada, S. 2008, *Journal of Physics G: Nuclear and Particle Physics*, 35, 085201, doi: [10.1088/0954-3899/35/8/085201](https://doi.org/10.1088/0954-3899/35/8/085201)
- Ji, F., Hu, J., Bao, S., & Shen, H. 2019, *Physical Review C*, 100, 045801
- Lattimer, J. M., Pethick, C. J., Prakash, M., & Haensel, P. 1991, *Physical Review Letters*, 66, 2701, doi: [10.1103/PhysRevLett.66.2701](https://doi.org/10.1103/PhysRevLett.66.2701)
- Lattimer, J. M., & Swesty, F. D. 1991, *Nuclear Physics A*, 535, 331, doi: [https://doi.org/10.1016/0375-9474\(91\)90452-C](https://doi.org/10.1016/0375-9474(91)90452-C)

- Maruyama, T., Chiba, S., Schulze, H.-J., & Tatsumi, T. 2007, *Physical Review D*, 76, 123015, doi: [10.1103/PhysRevD.76.123015](https://doi.org/10.1103/PhysRevD.76.123015)
- Miller, M. C., Lamb, F. K., Dittmann, A. J., et al. 2019, *The Astrophysical Journal Letters*, 887, L24, doi: [10.3847/2041-8213/ab50c5](https://doi.org/10.3847/2041-8213/ab50c5)
- . 2021, *The Astrophysical Journal Letters*, 918, L28, doi: [10.3847/2041-8213/ac089b](https://doi.org/10.3847/2041-8213/ac089b)
- Most, E. R., Weih, L. R., Rezzolla, L., & Schaffner-Bielich, J. 2018, *Physical Review Letters*, 120, 261103, doi: [10.1103/PhysRevLett.120.261103](https://doi.org/10.1103/PhysRevLett.120.261103)
- Nagakura, H., Furusawa, S., Togashi, H., et al. 2019, *The Astrophysical Journal Supplement Series*, 240, 38, doi: [10.3847/1538-4365/aafac9](https://doi.org/10.3847/1538-4365/aafac9)
- Nakazato, K., & Suzuki, H. 2019, *The Astrophysical Journal*, 878, 25, doi: [10.3847/1538-4357/ab1d4b](https://doi.org/10.3847/1538-4357/ab1d4b)
- Oertel, M., Hempel, M., Klähn, T., & Typel, S. 2017, *Reviews of Modern Physics*, 89, 015007, doi: [10.1103/RevModPhys.89.015007](https://doi.org/10.1103/RevModPhys.89.015007)
- Raduta, A., & Gulminelli, F. 2019, *Nuclear Physics A*, 983, 252, doi: <https://doi.org/10.1016/j.nuclphysa.2018.11.003>
- Riley, T. E., Watts, A. L., Bogdanov, S., et al. 2019, *The Astrophysical Journal Letters*, 887, L21
- Riley, T. E., Watts, A. L., Ray, P. S., et al. 2021, *The Astrophysical Journal Letters*, 918, L27
- Schneider, A. S., Roberts, L. F., & Ott, C. D. 2017, *Physical Review C*, 96, 065802, doi: [10.1103/PhysRevC.96.065802](https://doi.org/10.1103/PhysRevC.96.065802)
- Schneider, A. S., Roberts, L. F., Ott, C. D., & O'Connor, E. 2019, *Physical Review C*, 100, 055802, doi: [10.1103/PhysRevC.100.055802](https://doi.org/10.1103/PhysRevC.100.055802)
- Shen, G., Horowitz, C. J., & O'Connor, E. 2011a, *Physical Review C*, 83, 065808, doi: [10.1103/PhysRevC.83.065808](https://doi.org/10.1103/PhysRevC.83.065808)
- Shen, H., Ji, F., Hu, J., & Sumiyoshi, K. 2020, *The Astrophysical Journal*, 891, 148, doi: [10.3847/1538-4357/ab72fd](https://doi.org/10.3847/1538-4357/ab72fd)
- Shen, H., Toki, H., Oyamatsu, K., & Sumiyoshi, K. 1998a, *Progress of Theoretical Physics*, 100, 1013
- . 1998b, *Nuclear Physics A*, 637, 435
- . 2011b, *The Astrophysical Journal Supplement Series*, 197, 20, doi: [10.1088/0067-0049/197/2/20](https://doi.org/10.1088/0067-0049/197/2/20)
- Steiner, A. W., Hempel, M., & Fischer, T. 2013, *The Astrophysical Journal*, 774, 17, doi: [10.1088/0004-637X/774/1/17](https://doi.org/10.1088/0004-637X/774/1/17)
- Sumiyoshi, K., Kojo, T., & Furusawa, S. 2023, *Equation of State in Neutron Stars and Supernovae* (Springer Nature Singapore), 1–51, doi: [10.1007/978-981-15-8818-1_104-1](https://doi.org/10.1007/978-981-15-8818-1_104-1)
- Sumiyoshi, K., Nakazato, K., Suzuki, H., Hu, J., & Shen, H. 2019, *The Astrophysical Journal*, 887, 110, doi: [10.3847/1538-4357/ab5443](https://doi.org/10.3847/1538-4357/ab5443)
- Togashi, H., Nakazato, K., Takehara, Y., et al. 2017, *Nuclear Physics A*, 961, 78. <https://dx.doi.org/10.1016/j.nuclphysa.2017.02.010>
- Typel, S., & Alvarado Terrero, D. 2020, *The European Physical Journal A*, 56, 160, doi: [10.1140/epja/s10050-020-00172-2](https://doi.org/10.1140/epja/s10050-020-00172-2)
- Typel, S., Oertel, M., & Klähn, T. 2015, *Physics of Particles and Nuclei*, 46, 633
- Typel, S., Oertel, M., Klähn, T., et al. 2022, *The European Physical Journal A*, 58, 221. <https://compose.obspm.fr/>
- Weber, F., Farrell, D., Spinella, W. M., et al. 2019, *Universe*, 5, 169. <https://dx.doi.org/10.3390/universe5070169>
- Yasin, H., Schäfer, S., Arcones, A., & Schwenk, A. 2020, *Physical Review Letters*, 124, 092701, doi: [10.1103/PhysRevLett.124.092701](https://doi.org/10.1103/PhysRevLett.124.092701)
- Yasutake, N., Lastowiecki, R., Benić, S., et al. 2014, *Physical Review C*, 89, 065803, doi: [10.1103/PhysRevC.89.065803](https://doi.org/10.1103/PhysRevC.89.065803)
- Zhang, Z., & Chen, L.-W. 2013, *Physics Letters B*, 726, 234, doi: <https://doi.org/10.1016/j.physletb.2013.08.002>